

Multidimensional Modelling of Cross-Beam Energy Transfer for Direct-Drive Inertial Confinement Fusion

(Hopefully soon to be Dr.) Philip W. X. Moloney

IMPERIAL

June 2024

Submitted in partial fulfilment of the requirements for the degree of
Doctor of Philosophy of Imperial College London

Department of Physics
Imperial College London
Prince Consort Road
London SW7 2AZ

Contents

1	Introduction	7
1.1	Nuclear Fusion	7
1.2	Inertial Confinement Fusion	10
1.2.1	Ignition Requirements	10
1.2.2	Central Hotspot Ignition	12
1.2.3	Alternative Ignition Approaches	14
1.2.4	Inertial Fusion Energy Considerations	15
1.3	Current Experiments/ Main Approaches	16
1.3.1	Indirect-Drive	16
1.3.2	Direct-Drive	19
1.4	Objective of the work	23
	Bibliography	27
	Copyright Permissions	35

List of Acronyms

MHD Magnetohydrodynamics

Rad-Hydro Radiative-Hydrodynamics

LPIs Laser-Plasma Instabilities

CBET Cross-Beam Energy Transfer

ICF Inertial Confinement Fusion

SBS Stimulated Brillouin Scattering

SRS Stimulated Raman Scattering

TPD Two Plasmon Decay

EPW Electron Plasma Wave

LLE Laboratory for Laser Energetics

LLNL Lawrence Livermore National Laboratory

CEA Commissariat à l'Énergie Atomique et aux Energies Alternatives

EPW Electron Plasma Wave

Inv-Brem Inverse-Bremsstrahlung

RTI Rayleigh–Taylor Instability

NIF National Ignition Facility

LCOE Levelised Cost of Electricity

MCF Magnetic Confinement Fusion

IFE Inertial Fusion Energy

DPSSL Diode-Pumped Solid State Laser

LMJ Laser Mégajoule

LEH Laser Entrance Hole

HDC High Density Carbon

SSD Smoothing by Spectral Dispersion

1 Introduction

1.1 Nuclear Fusion

Nuclear fusion is a reaction which combines multiple light nuclei together to form heavier nuclei. If the products of the reaction are more tightly bound than the reactants, excess energy is also released to the products. Broadly, the binding energy per nucleon of common nuclear isotopes increases with atomic mass up to iron, ^{56}Fe , and decreases afterwards, as is shown in Fig. 1.1. The reverse process, nuclear fission, operates by splitting heavy nuclei into lighter products. Therefore, Energy is mostly released via fusion, up to product masses including iron, and via fission down to iron. In 2023, fission made up approximately 9.1% of the global electricity mix [1]. Like fission, fusion energy would be carbon free at the point of production, but it would also offer further distinct advantages. Fusion power plants would not operate in regimes with potentially dangerous chain reactions, and would also generate little-to-no long-lived nuclear waste. In comparison with other low-carbon power sources, including wind and solar, fusion plants could operate continuously, supplying base load power. Studies have also shown that fusion energy could have an economically viable Levelised Cost of Electricity (LCOE), which is a metric that compares the economic costs of a power plant over its lifetime to the value of energy produced [2]. Performing controlled nuclear fusion on Earth for energy production has been an active area of research for many decades. However, multiple scientific and engineering challenges remain to be resolved, in order to make it a viable energy source.

The likelihood of two reactants undergoing a specific fusion reaction is described by the cross-section of the interaction,

$$\sigma(E) = \frac{S(E)}{E} e^{-E_G/E}, \quad (1.1)$$

which is a function of the centre of mass energy, E , the ‘astrophysical S -factor’, $S(E)$, which is a weakly varying function of energy for many reactions, and the Gamow Energy, E_G [3]. The exponential term including E_G in Eq. 1.1 is related to the probability of reactants tunnelling through the energy barrier, due to electrostatic Coulomb repulsion between two positively charged reactant nuclei. One approach to achieving the energies required to overcome this barrier are ‘beam-target’ configurations, wherein a high energy beam of reactants is focussed onto a stationary target. However, this has proven unviable, due to the high likelihood of Coulomb scattering events compared to fusion reactions [4]. Thermonuclear fusion is the alternative approach, wherein the bulk fuel is heated to sufficient temperatures that the particles in the high-energy tail of the distribution have sufficient energy to undergo fusion reactions. For a fuel is in thermal equilibrium, the high particle energies required to overcome

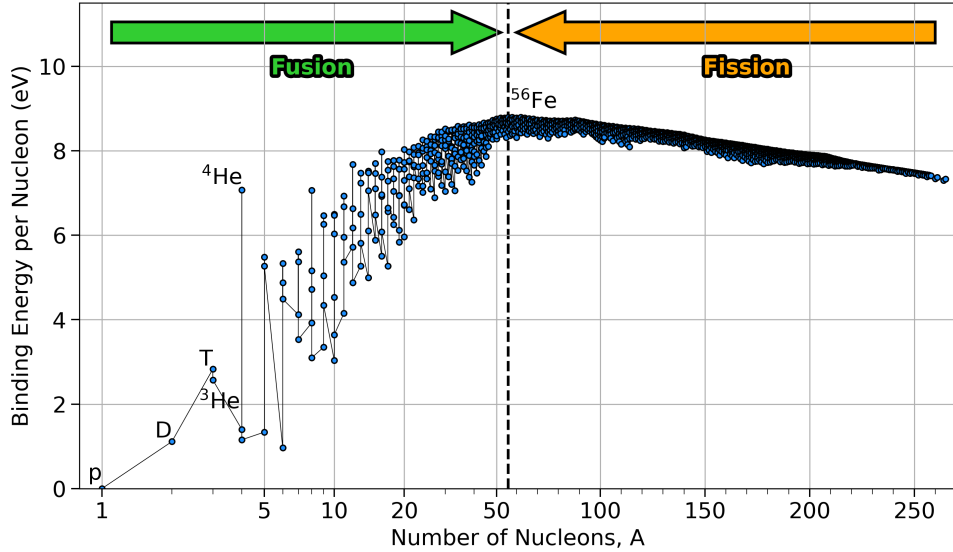


Figure 1.1: Binding energy per nucleon for common nuclear isotopes. Binding energy peaks close to iron, and energy is released for reactions which increases binding energy of the products compared to the reactants. ${}^4\text{He}$ has a particularly high binding energy and therefore fusion reactions which results in this isotope are strong candidates for fusion energy production.

the Coulomb barrier, $\mathcal{O}(100)$ keV, are well above ionisation energies (e.g. 13.6 eV for hydrogen), so the fuel will be in the plasma state. If the fusion products are able to deposit a sufficient fraction of their energy back into the fuel, then a self-sustaining fusion reaction is possible, where the high temperatures required for the reactants to fuse is maintained. For a fusion reaction with reactants labelled by 1 and 2, the number of fusion reactions per unit time and volume is known as the ‘volumetric reaction rate’ [3],

$$R_{12} = \frac{n_1 n_2}{1 + \delta_{12}} \langle \sigma v \rangle, \quad (1.2)$$

where v is the relative velocity of a pair of reactants, δ_{12} is the Kronecker delta, which accounts for double counting of species and the ‘averaged reactivity’ $\langle \sigma v \rangle$ is defined as the integral over the velocity distribution,

$$\langle \sigma v \rangle \equiv \int_0^\infty \sigma(E) v f(v) dE. \quad (1.3)$$

Eq. 1.2 explicitly demonstrates that achieving a high fuel density, can significantly enhance reaction rates, due to the square dependence on number density.

The efficacy of a fusion fuel for energy production is dictated by the availability of the reactants, the fusion products, the averaged reactivity of the reactants and the energy released per reaction, Q , which is the difference in binding energy between the reactants and products. Most current, fusion-energy experiments are focussed on demonstrating that fusion power production is possible, thus the choice of fuel is predominantly dictated by the reac-

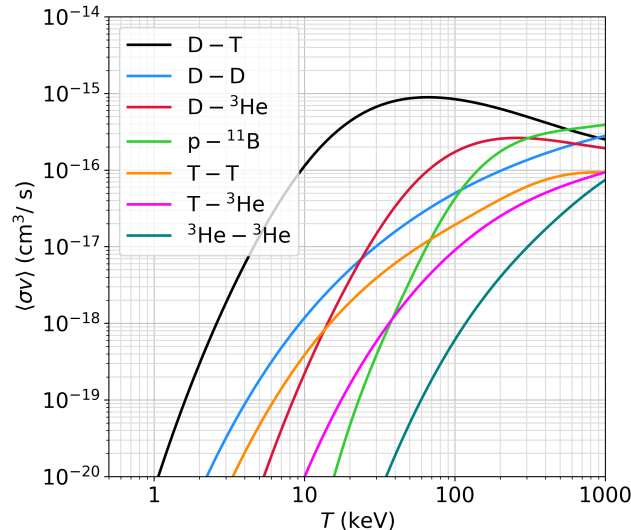


Figure 1.2: Averaged reactivities for important fusion reactions. The deuterium-tritium reactivity is significantly larger than all other reactions up to $T \sim 500$ keV. Averaged reactivities are obtained from cross-section data, available in the ENDF/B-VII.1 library [5].

tivity. Hydrogen-Hydrogen isotope fusion reactions have much higher reactivities than other elements, because the Coulomb repulsion scales as Z^2 , thus the Gamow energy, E_G is significantly smaller. The nuclear physics is particularly favourable for the fusion of deuterium (D) and tritium (T). This is due to a nuclear resonance at relatively modest energies for the reaction chain which produces an excited, unstable ${}^5\text{He}$ nucleus, that subsequently decays to ${}^4\text{He}$ and a neutron [6]. Averaged-reactivities of several important fusion reactions, obtained from reaction cross-sections from the ENDF/B-VII.1 library [5], are plotted in Fig. 1.2. The D-T reactivity is at least an order of magnitude larger than the other reactions plotted, up to $T \sim 100$ keV, and it is thus the most commonly used fuel for high-gain fusion experiments. The reaction proceeds as,



where α is a ${}^4_2\text{He}$ nucleus, which gains 3.5 MeV from the fusion energy released, Q , and n is a neutron, which gains 14.1 MeV. The energy partition is dictated by energy-momentum conservation of the products in the centre of mass frame. The alpha particles typically couple their energy back into the bulk fuel via Coulomb collisions, which has the effect of raising the fuel temperature and thus further raising the reactivity, at temperatures below $T \sim 60$ keV. Neutrons have a much lower reaction cross-section because they are not charged, and thus typically leave the reaction region. However, in fusion experiments with high density configurations such as Inertial Confinement Fusion (ICF), neutron heating of the fuel can also play a significant role [7].

In order for net energy gain, sufficient energy must be released by fusion to compensate for the energy required to perform the experiment. This requires a fuel configuration with a

combination of high temperatures and densities to obtain a large volumetric reaction rate. It must also remain confined for a sufficient time for enough reactions to occur to result in net energy gain. The method of confinement for fusion energy experiments has two broad streams: Magnetic Confinement Fusion (MCF), where magnetic fields are used to confine steady-state fusion-plasma over long time-scales [8], and ICF, where dense fusion fuel is assembled for a short time period and ‘confined’ by its own inertia [9]. The work conducted in this thesis is of relevance to ICF schemes, specifically those in which the plasma is produced by laser irradiation.

1.2 Inertial Confinement Fusion

Large energy releases from nuclear fusion have been achieved on Earth in the form of nuclear warheads, although quantity of energy released in these uncontrolled reactions would destroy any infrastructure which would attempt to harness the power for energy production. In the 1950s and 60s, the first devices were built which demonstrated stimulated emission of microwave [10] and optical [11] light. The optical-wavelength lasers were quickly recognised as an ideal driver for a far smaller and therefore less destructive thermonuclear device than was used in warheads, which could thus be used for fusion energy generation [12]. Much of the research was declassified and subsequently published in an article by Nuckolls *et al.* in 1972 [9]. In these ICF experiments, the high temperatures and densities required to initiate an appreciable number of fusion reactions are maintained over a short timescale, which is set by the inertia of the fuel configuration, before the fuel disassembles due to large pressure gradients. The required fuel density is typically achieved by an implosion process. High temperatures are obtained either from the conversion to internal energy of the implosion kinetic energy, which is the central hotspot ignition variant, described in Sec. 1.2.2, or via an external heating source, as described in Sec. 1.2.3. Before describing these schemes in more detail however, necessary criterion for energy gain conditions shall be discussed, which are agnostic of how the fusion fuel is assembled and dictate the plasma conditions which must be achieved.

1.2.1 Ignition Requirements

The point at which alpha heating becomes the dominant term in the power balance of the fusion fuel is termed ‘ignition’ and it is a necessary, although not sufficient condition for high gain ICF experiments. Ignition necessitates that the plasma is confined for a sufficiently long period of time, for an appreciable number of fusion reactions to occur, raising the fuel temperatures and reactivities, which results in propagating fusion burn. Estimates for the required plasma conditions which must be achieved for this to occur, can be estimated by considering the timescales of confinement and fusion. Initially, a uniform ion number density n_i and temperature T , spherical fuel assembly, with outer radius R , shall be considered. The ions have an average mass, m_i , such that the mass-density of the fuel, $\rho = m_i n_i$ and the volume of the fuel sphere, $V = 4\pi R^3/3$. Dimensional considerations give an order of

magnitude estimate for the timescale on which fusion reactions occur,

$$\tau_{\text{fus}} = \frac{1}{n_i \langle \sigma v \rangle}. \quad (1.5)$$

A radially inward pressure gradient will exist due to the high temperature of the plasma, which will lead to an inward propagating rarefaction wave, disassembling the fuel. This rarefaction wave will move at the isothermal sound speed, $c_s = \sqrt{2k_B T / m_i}$,¹ from $t = 0$, such that its position of the wave is given by $r = R - c_s t$. Therefore, the timescale on which the burning fuel remains un-rarefied and thus confined is,

$$\begin{aligned} \tau_{\text{conf}} &= \int_0^{R/c_s} \frac{(R - c_s t)^3}{R^3} dt, \\ &= \frac{R}{4c_s}. \end{aligned} \quad (1.6)$$

The ratio of these timescales,

$$\frac{\tau_{\text{conf}}}{\tau_{\text{fus}}} = \frac{\langle \sigma v \rangle \rho R}{4m_i c_s}, \quad (1.7)$$

illustrates that, for ignition and hence gain, ICF reactions require a large ρR value, which is typically referred to as the ‘areal-density’ [13].

The timescale ratio can be used to derive the ‘burn-up fraction’, which is defined as the ratio of fusion reactions, $N_{\text{fus}} = R_{\text{DT}} V \tau_{\text{conf}}$, to the number of DT pairs, $N_{\text{DT}} = n_i / 2$, in the fuel assembly,

$$\begin{aligned} \Phi &\equiv \frac{N_{\text{fus}}}{N_{\text{DT}}}, \\ &= \frac{\rho R}{H_B}, \end{aligned} \quad (1.8)$$

where the ‘burn-parameter’, $H_B \equiv \langle \sigma v \rangle / 8m_i c_s$ has been defined, which is simply a function of temperature and should be minimised to achieve the highest Φ possible. For DT fuel, there is a minimum of the burn-up parameter, $H_{B,\min} \sim 7 \text{ g/cm}^2$, which occurs at $T \sim 40 \text{ keV}$ [3]. Low temperatures raise H_B due to low reactivities, and high temperatures increase H_B by increasing the rate of fuel disassembly rates due to increased rarefaction wave speeds. Eq. 1.8 is only valid for $\Phi \ll 1$, because the conversion of DT pairs into non-fusing products has not been considered. A modified form of Eq. 1.8, which approximately accounts for burn-depletion, was derived by Fraley *et al.* in Ref. [13],

$$\Phi = \frac{\rho R}{H_B + \rho R}. \quad (1.9)$$

Using the approximate minimum $H_{B,\min} \sim 7 \text{ g/cm}^2$ in Eq. 1.9, suggests that a burn-up fraction of $\Phi = 30\%$ can be achieved with an areal density, $\rho R = 3 \text{ g/cm}^3$. If solid density DT was used, the mass of fuel required to achieve $\Phi = 30\%$ of the fuel would be 2.5 kg, which would release the same energy as 50 kilotons of TNT [14]. In order to harness the released

¹The factor of 2 in c_s is because the pressure is the sum of contributions from ions and electrons.

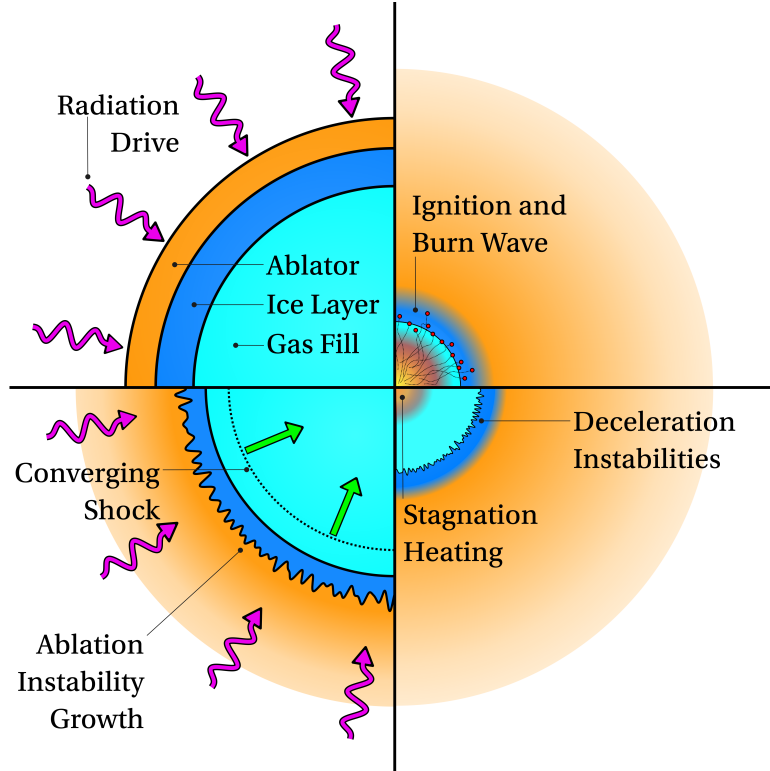


Figure 1.3: Four key Stages of the central hotspot ignition ICF concept. The chronological order of the diagram is top-left, bottom-left, bottom-right and then top-right quadrants, which display the initial configuration, implosion, stagnation and burn propagation stages respectively.

fusion energy without destroying the surrounding infrastructure, a smaller energy release and therefore mass is required, which necessitates compression of the fuel to achieve the ρR constraint. A pellet containing 1 mg, compressed to densities $\mathcal{O}(10^3)$ times solid density, could release 100 MJ of fusion energy at $\Phi = 30\%$. Spherical compression is optimal because the fuel compresses in three dimensions. This minimises the required convergence ratio, $CR = R_{\text{init}}/R_{\text{final}}$, which increases the tolerance to hydrodynamic instabilities.

1.2.2 Central Hotspot Ignition

Increasing the fuel mass in an ICF experiment requires larger and larger driver energy to heat the entire fuel to the required fusion temperatures, $T \sim 5$ keV. This necessitates larger and more expensive drivers, limiting both the upfront driver cost and potential target gain. Therefore, experimental configurations which can minimise the driver energy required to ignite a given fuel mass are more practical for current experiments and future power plants. The ‘central hotspot ignition’ method is one such configuration, where a thin shell of fuel containing a low density fuel-fill is approximately isentropically compressed by a carefully constructed driver pulse shape. Isentropic compression maintains a cold and dense, imploding fuel shell, while compressing the gas fill. Only a small mass of fuel is heated to the required fusion temperatures on the stagnation axis. The energy required for this heating is provided from implosion kinetic energy of the dense shell, which transfers this energy to the

gas analogously to a stiff piston compressing a gas. Fig. 1.3 shows a schematic representation of a central hotspot ignition implosion at 4 important stages. The top left quadrant shows the initial, spherical target configuration, which is comprised of an outer ablator, a solid DT ice layer and an inner DT gas fill. Choice of ablator material is driven by a number of considerations, including mass ablation rate, minimisation of instability growth, radiation coupling and ease of manufacturing [15, 16, 17, 18]. Cryogenic temperatures are required to form the ice layer from the DT fuel. The driver should, ideally, uniformly irradiate the outer surface to maintain the optimal spherical compression and to minimise instability growth. Specific radiation drives shall be discussed in Sec. 1.3, but for now, the scheme shall be discussed, while remaining agnostic of the driver.

The bottom left quadrant of Fig. 1.3 shows the implosion phase of the scheme. As the radiation from the driver heats the outer layer of the ablator, it heats up and expands radially outward, which imparts a rocket force on the interior target, propelling it inward. A low density gas fill is used to make compression of the target easier such that high convergence ratios can be achieved. Greatest convergence can be achieved if the pressure of the gas fill is minimised and thus high-gain ICF targets aim to limit ‘preheat’ of the interior gas fill ahead of the shock. For example, a poorly pulse-shaped driver will lead to undesired shock heating of the interior fuel ahead of the converging shell, which raises its pressure and thus limits compressibility. Assuming perfectly spherical targets and driver radiation, isentropic pulses maximise the target gains, which are designed to limit shock preheating of the gas-fill. In reality, target defects and short wavelength perturbations in the driver radiation seed the Rayleigh–Taylor Instability (RTI) on the ablation surface, which can grow due to the misaligned density and pressure gradients. Realistic pulse shapes often slightly preheat the target, which increases stability to hydrodynamic instability growth [19, 20]. The preheat and thus stability of the design, is typically parameterised by the ‘adiabat’ parameter,

$$\alpha = \frac{P_{\text{shell}}}{P_{\text{F}}}, \quad (1.10)$$

where P_{shell} is the pressure of the DT shell and P_{F} is the Fermi degenerate pressure, *i.e.* truly isentropic compression of a $T \sim 0$ K fuel has $\alpha = 1$. Higher adiabat designs are more stable, and the parameter is set in each shot by launching a weak shock through the capsule before the main pulse.

The stagnation phase of the implosion is shown in the bottom right quadrant of Fig. 1.3. As the remaining relatively cold and dense shell converges on the axis, PdV heating raises the temperature of the compressed interior gas fill. If the implosion velocity is sufficiently high, this piston heating of the fuel results in fusion relevant temperatures. The deceleration phase is also hydrodynamically unstable, because the high pressure, low density interior pushes on the high density, low pressure shell, which results in further RTI growth. Long wavelength perturbations to the radiation drive result in unstaginated kinetic energy in the hotspot, limiting maximum achievable temperatures [21]. Short wavelength perturbations from the RTI, can introduce high-Z ablator material to the hotspot which enhances radiative losses. If the perturbations are sufficiently large amplitude, they can puncture the shell,

severely degrading confinement [22].

The upper-right quadrant of Fig. 1.3 shows the final, ignition and burn propagation phase of the design. If the density and temperature of the fuel hotspot are sufficient, then fusion reactions begin to occur, generating energetic alpha fusion products. For sufficiently high areal density shells, the alpha particles deposit their energy in the dense fuel shell, raising its temperature and ablating additional fusion fuel radially inward to the burn process. This leads to ignition, if the confinement holds the fuel together for a sufficiently long period of time.

1.2.3 Alternative Ignition Approaches

In the central hotspot ignition scheme, the energy required to heat the fuel to fusion temperatures is supplied by the kinetic energy of the imploding shell. The high shell velocities required to obtain hotspot fusion temperatures is ~ 300 km/s, which is typically large enough to result in significant instability growth. Alternative schemes exist, namely the shock- and fast-ignition variants, where the required shell density is obtained via a much slower implosion process, limiting instability growth. Temperatures are then achieved by applying a heating source, separate from the implosion dynamics. For shock ignition, the driver pulse shape is sharply ramped up at the end of the pulse, in order to generate a strong, spherically converging shock, heating the fuel to fusion temperatures [23, 24]. The main issue with this scheme for laser-driven ICF, has been questions over laser coupling at the high intensities required to generate the ignitor shock. At high laser intensities, a mostly deleterious class of laser-plasma interaction known as Laser-Plasma Instabilities (LPIs) dominate. Recent work has explored the possibility of augmenting the laser pulse shape to add a dip in power, prior to the ignitor pulse rise, which conditions the plasma such that it is more amenable to strong shock generation, and thus limits the intensities required [25].

Fast-ignition is an alternative concept which utilises an external ignitor-beam of charged particles, to provide the hotspot heating [26]. Scientific research related to this scheme include studying how the high energy charged particles are generated via ultra-intense laser interactions, and if they can be focused to efficiently couple their energy to the fuel [27, 28]. The overall complexity of many of proposed driver and target configurations would also likely have to be reduced, in order to make Inertial Fusion Energy (IFE) relevant targets.

All of the ignition concepts introduced so far focus on igniting a small central mass, which then initiates a propagating burn wave into surrounding fuel. The volume-ignition variant, instead proposes igniting the entire fuel volume simultaneously [29, 30]. This is achieved by assembling a large, dense fuel mass, kept at a much lower temperature than the hotspot in other schemes. A large and dense fuel assembly has minimal radiative losses and can thus ignite at $T \sim 1.5$ keV, as opposed to the ideal ignition temperature of hotspot schemes, $T = 4.3$ keV [3]². One issue with this scheme is that significantly more laser energy is required to ignite a given fuel mass, because the entire volume must be brought to ignition conditions at the same time.

²The ideal ignition temperature is the value at which alpha heating balances radiative losses.

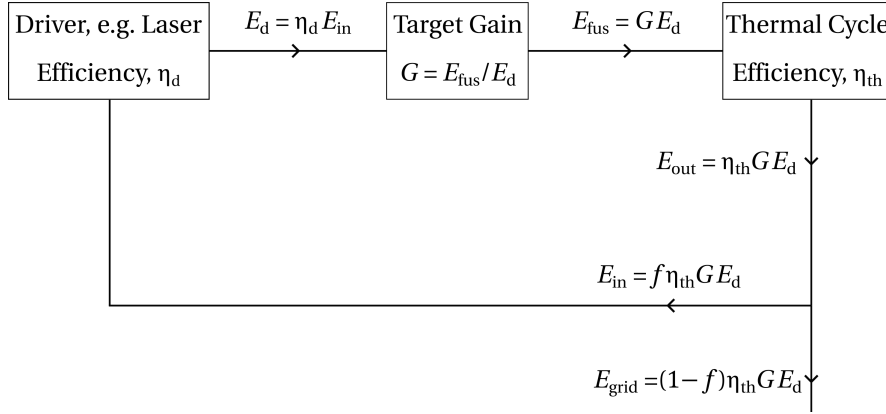


Figure 1.4: Energy balance of an IFE power plant. Based on a similar figure from Ref. [3].

1.2.4 Inertial Fusion Energy Considerations

For a power plant to produce net energy from ICF implosions, the energy from each target must of course be greater than the energy to drive the implosion. In reality, additional inefficiencies in power plants set more stringent constraints on the energy which must be produced. The energy balance of an IFE power plant is shown in Fig. 1.4. A driver, such as a laser system (which is the driver considered for the work conducted in this thesis), converts an input energy, E_{in} , to a driver energy, $E_d = \eta_d E_{\text{in}}$, where η_d is the energy efficiency of the driver. The driver energy initiates a fusion reaction, which releases E_{fus} , with a gain defined by,

$$G = E_{\text{fus}}/E_d. \quad (1.11)$$

The released fusion energy, for example in the form of energetic neutrons, is converted into thermal energy in an encompassing ‘blanket’, and then into output electrical energy, E_{out} , by a thermal-cycle (such as steam turbines), with efficiency, η_{th} . Some fraction f of this generated energy is recycled back into the plant to power the driver, such that the remaining fraction is sent to the grid,

$$E_{\text{grid}} = (1 - f)\eta_{\text{th}}\eta_d G E_{\text{in}}, \quad (1.12)$$

with the constraint, $f\eta_{\text{th}}\eta_d G \geq 1$ for net energy production. Power plants must also produce a sufficiently large volume of energy to be economical. Therefore, several ~ 100 MJ reactions must occur each second for a 100 MW plant, which necessitates a driver that can operate at ~ 10 Hz.

The Diode-Pumped Solid State Laser (DPSSL) concept, could feasibly produce laser energy at ~ 10 Hz repetition rate, with an efficiency $\eta_d \sim 10\%$ [31, 32]. Assuming a thermal cycle efficiency, $\eta_{\text{th}} = 40\%$ and a recycled energy fraction, $f = 1/4$, this means that a target gain of approximately $G \sim 100$ would be required for power production. Additionally, the plant must be economically profitable, thus for a $G = 100$ reaction, which releases $E_{\text{fus}} = 100$ MJ = 28 kWh, the energy sold to the grid would make about £1.50³. Therefore, targets must cost approximately £0.10, which limits the tolerable manufacturing complexity. IFE target concepts exist,

³The UK April 2024 energy price of £0.25 per kWh was used.

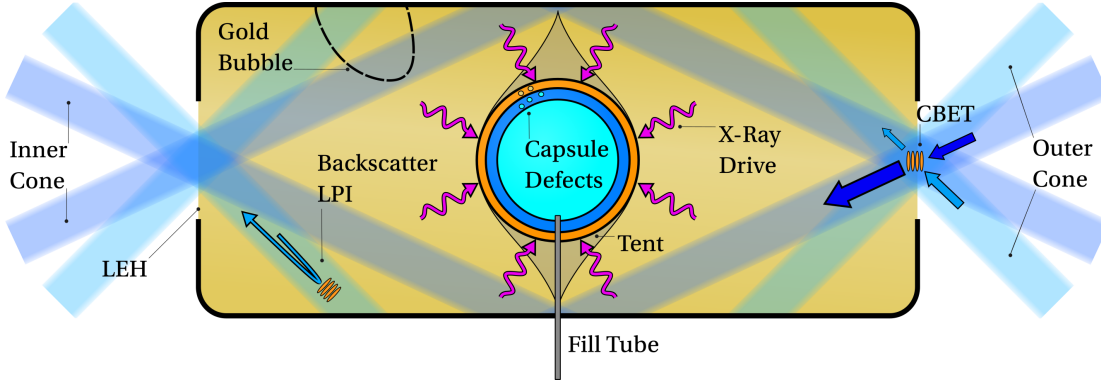


Figure 1.5: Schematic of the indirect-drive approach to ICF. Laser light, represented as blue transparent rectangles, irradiates the interior of a high-Z (e.g. gold) hohlraum, producing thermal x-rays that drive the capsule implosion. A number of important physical effects, typical to indirect-drive experiments, are also illustrated on the diagram.

which could feasibly be mass-produced for an acceptable cost, for example initially uniform density liquid spheres, known as ‘dynamic shell’ targets [33, 34].

1.3 Current Experiments/ Main Approaches

In Sec. 1.2, the basic principles of ICF were introduced without specifying the driver technology. Although heavy ion beams have been proposed as a driver technology [35], most current research focusses on the direct-drive and indirect-drive approaches, which use laser light to directly and indirectly irradiate the target respectively. For the direct-drive approach, lasers are focussed upon the outer surface of the target, whereas in indirect-drive, they illuminate the interior surface of a high-Z material ‘hohlraum’, which generates a thermal bath of x-rays. The indirect-drive approach was developed in order to relax requirements on laser beam uniformity and sensitivity to hydrodynamic instabilities in direct-drive [36]. Sources of degradation and implosion dynamics are somewhat different in each of these approaches. Each approach is introduced below, and progress on the main experimental facilities is summarised.

1.3.1 Indirect-Drive

1.3.1.1 Indirect-Drive Physics

A schematic of an indirect-drive experiment is shown in Fig. 1.5. The National Ignition Facility (NIF) at the Lawrence Livermore National Laboratory (LLNL) in the United States of America, is the largest ICF facility and high power laser system in the world, and it mainly focusses on the indirect-drive approach to ICF [37, 38]. The laser system is composed of 192 beams, which are clustered around two poles, so that they can enter the small Laser Entrance Hole (LEH) of the hohlraum, as is demonstrated in Fig. 1.5. Approximately 2 MJ of laser energy can be delivered to the target, usually on a timescale of $10 \rightarrow 20$ ns. The Laser

Mégajoule (MJ) is a newer facility at Commissariat à l'Énergie Atomique et aux Energies Alternatives (CEA) in France, which is the largest ICF experiment outside the United States. It also predominantly focusses on the indirect-drive approach and, although currently still in construction, it is intended to have 176 beams that will deliver approximately 1 MJ of laser energy to the hohlraum [39].

The main benefit of the indirect-drive approach compared to direct-drive is the uniformity of the driving radiation. High power laser focal spots are instantaneously highly non-uniform, which is discussed in more detail in Sec. 1.3.2. This can seed instabilities and target compression is also limited based on the number of available beams. Conversion of laser light to x-rays in a hohlraum creates a highly uniformly radiation field, which has limited short wavelength perturbations to seed RTI growth. Instability growth is therefore mostly seeded from engineering features, such as the tent used to hold the capsule in place, defects in the capsule, surface roughness, and the fill tube used to insert the fuel [40]. A high-Z material such as gold is used for the hohlraum, due to high laser absorption and emissivity. Longer wavelength modes can be seeded if the laser heating of the hohlraum is asymmetric. For example, Fig. 1.5 shows that the hohlraum wall can heat and expand, blocking the ‘inner-cone’ beams which heat the material near the capsule equator. Filling the hohlraum with a low-Z gas fill⁴ to limit the ‘gold bubble’ expansion, however, this allows for deleterious LPIS to occur, which reflect laser energy back out of the LEH [41]. Current experiments on the NIF, use a relatively low gas fill to reduce backscatter-LPIs (specifically Stimulated Brillouin Scattering (SBS) and Stimulated Raman Scattering (SRS)), and introduce a wavelength shift between the inner and outer cones of laser beams, which allows for a laser-plasma interaction known as Cross-Beam Energy Transfer (CBET) to transfer power to the outer beams late in the implosion[42, 43, 44]. This compensates for absorption in the expanding gold bubble and can maintain symmetry of the implosion. The main drawback of the approach compared to the direct-drive, is that the conversion of laser light to capsule kinetic energy via the hohlraum, introduces an additional ~ 10% efficiency decrease, limiting the maximum gains that can be achieved. Increasing the size of the capsule relative to the hohlraum increases the fraction of x-ray energy which is coupled to the target, but can introduce long-wavelength instabilities if made too large by blocking laser propagation. Direct-drive is thus often considered the preferred scheme for IFE.

1.3.1.2 Indirect-Drive Experimental Progress

Although early experiments on the NIF dramatically underachieved the main aim of demonstrating ignition, a tremendous amount of progress has been made in recent years [46]. Fig. 1.6 plots G for indirect-drive ICF shots on the NIF, up to December 2022 [45]. The initial target designs, up to 2013, utilised a low adiabat design, with a plastic (CH) ablator, known as ‘Low Foot’, which proved very sensitive to hydrodynamic instabilities [47]. The results of this campaign are plotted in shaded grey in Fig. 1.6. This led to the subsequent, ‘High Foot’ campaign, where the target was kept similar, but the adiabat of the design was raised to create

⁴A low-Z hohlraum fill is used to limit laser absorption away from the hohlraum wall.

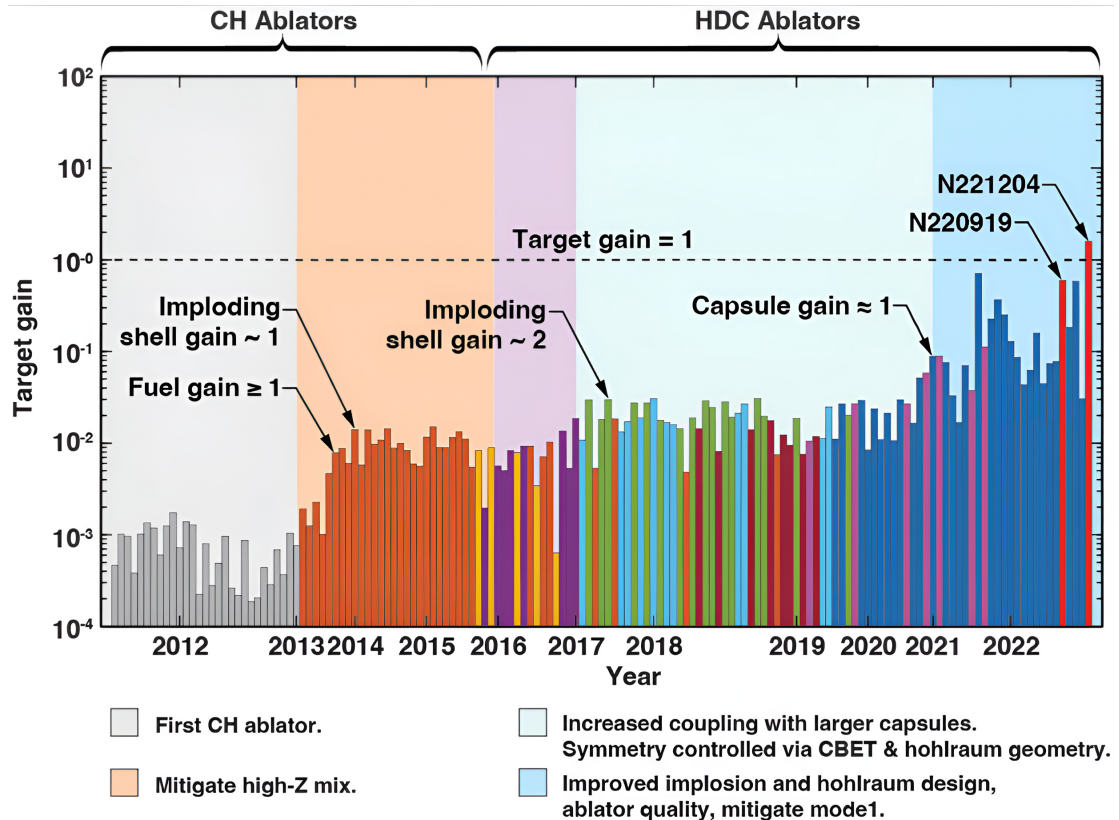


Figure 1.6: G plotted against time for indirect-drive ICF shots on NIF. The colour of each bar represents a different implosion design, and the dashed horizontal line represents $G = 1$, where the fusion energy produced is equal to the incident laser energy. Used under CC BY 4.0 from Ref. [45].

a more stable implosion, which improved yields, plotted in red [20]. A new ablator material, High Density Carbon (HDC), was deployed subsequent to this campaign which had a higher density than CH, resulting in improved absorption and thus shorter laser pulses [48]. The gas fill-density of the hohlraum was also lowered to reduce the loss of laser energy to backscatter LPIs. The ‘Hybrid’ campaigns made further improvements, by utilising CBET to compensate for the loss of symmetry resulting from the gold-bubble expansion in the low-fill hohlraum, using larger capsules to increase coupling efficiency and thicker shells to mitigate instabilities [49]. Additional improvements were made to capsule quality which minimised sources of instability [50]. Shots from these campaigns are shown in the light and darker blue in Fig. 1.6 and have led to experiments entering the burning-plasma⁵ [51, 52] and ignition regimes [53]. This ultimately resulted a shot $G > 1$ in December 2022, which was the first fusion experiment to produce more energy than the driver delivered [45]. Although not plotted in Fig. 1.6, the gain record at the time of writing stands at $G = 2.4$ [54].

⁵The burning-plasma regime is when alpha heating is larger than PdV heating. This is opposed to ignition, where alpha heating is greater than loss terms.

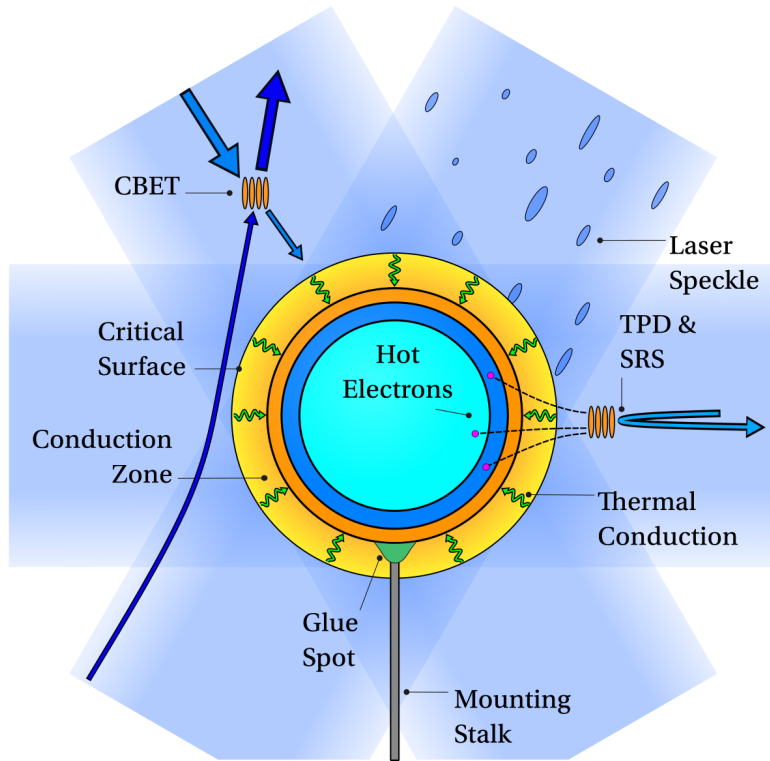


Figure 1.7: Schematic of the direct-drive approach to ICF. Laser light, represented by the transparent, blue rectangles is absorbed outside the critical surface and then transported in to the ablation surface by thermal conduction. Speckle from beam smoothing optics leads to short-scale non-uniformity of deposition, known as imprint. LPs degrade the performance, both by reflecting light, and by generating hot electrons which pre-heat the fuel.

1.3.2 Direct-Drive

1.3.2.1 Direct-Drive Physics

A schematic of a direct-drive experiment is shown in Fig. 1.7. Although a limited number of direct-drive implosions are performed on the NIF, the largest dedicated direct-drive facility in the world is the OMEGA laser facility at the Laboratory for Laser Energetics (LLE) in the United States [55, 56]. Work presented in this thesis is most relevant to direct-drive implosions on this facility. The OMEGA laser has a total of 60 beams, arranged to provide approximately symmetric radiation to a spherical target. In total, beams can deliver approximately 30 kJ of laser energy to the target, usually in a timescale of $2 \rightarrow 3$ ns. As previously stated, high driver efficiencies are desirable for IFE, and the relative inefficiency of the hohlraum light to x-ray conversion, means that direct-drive is the assumed method for a future IFE power plant. As opposed to indirectly-driven NIF experiments, where the capsule is held in place by a thin tent attached to the hohlraum, directly-driven OMEGA targets are glued to a mounting stalk to hold them in place initially. This can lead to low-mode asymmetries and unstagnated flows in the hotspot, which degrade the performance [57].

In plasmas, electro-magnetic radiation is absorbed beyond the critical surface, which is the surface interior to which the electron density is sufficiently high, that light of a given

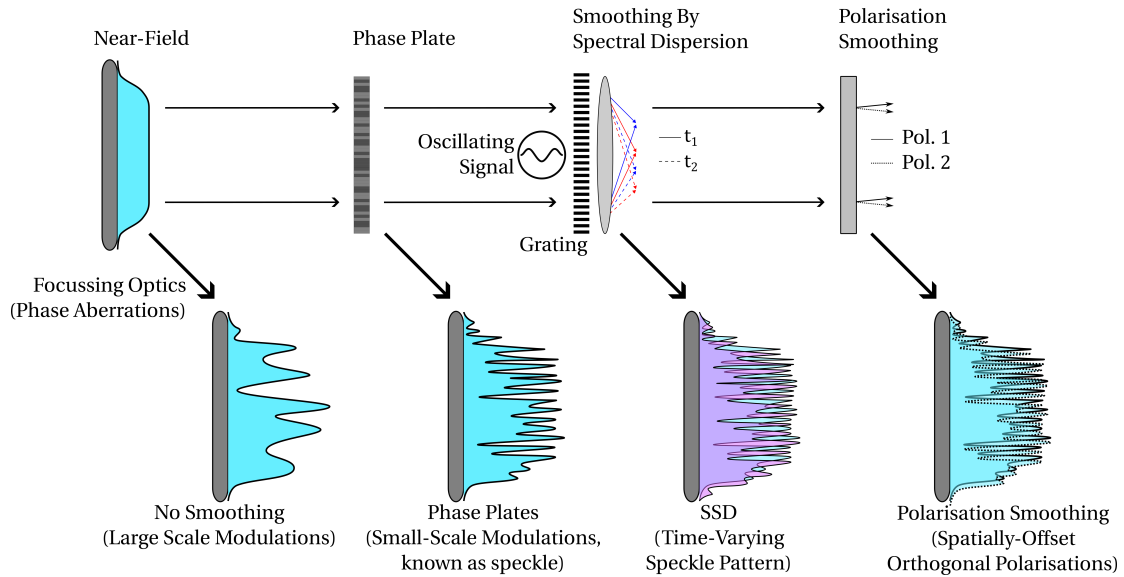


Figure 1.8: Schematic of beam smoothing techniques employed on the OMEGA laser system. Phase aberrations can lead to large scale modulations to the far-field intensity profile. Phase plates shift the perturbations to shorter scales, which are more efficiently smoothed by thermal conduction. Smoothing by Spectral Dispersion (SSD) creates a time-varying speckle pattern, which leads to a smooth, *time-integrated* far-field profile. Polarisation smoothing splits the beam into orthogonally polarised sub-beams, which do not interfere and thus further reduce non-uniformity.

wavelength cannot propagate. For indirect-drive, high frequency x-rays are absorbed close to the ablation surface, whereas for direct-drive, longer wavelength laser light has a critical surface which is exterior to the ablation surface. Thus, energy is absorbed beyond the critical surface, heating this ‘coronal plasma’⁶ to high temperatures. The absorbed laser energy is then transported radially inward via thermal conduction in the ‘conduction-zone’, to the higher density, lower temperature ablation surface, as is shown in Fig 1.7. Non-uniform absorption at the critical surface is partially smoothed by non-radial thermal conduction in this region, which is more efficient for shorter wavelength perturbations [58].

Despite this non-radial smoothing in the conduction zone, non-uniformity of the laser drive has proven to be a significant difficulty for direct-drive ICF implosions. The beam layout and their widths lead to a ‘beam-mode’ asymmetry, which for OMEGA has a distinctive Legendre-mode, $\ell = 10$ pattern, which can be seen in Fig. ???. Focal spots of high power lasers are also often highly non-uniform when so-called ‘beam-smoothing’ techniques are not employed. As light propagates from the beam port to the far-field, random ‘phase-aberrations’ are picked up by the beam due to distortions in the medium through which it travels. These then result in large scale modulations of the focal spot intensity profile. When the target is illuminated by these modulated beams, significant asymmetry is imparted on the drive, severely limiting the overall performance. A variety of beam smoothing techniques

⁶The term coronal plasma shall be used throughout this thesis to refer to the approximately isothermal, outward flowing, low density plasma blow-off, which is exterior to the critical surface.

are thus employed which lead to a significantly more uniform beam profile. Fig. 1.8 shows a schematic of several important beam smoothing techniques employed by the OMEGA laser system. The diagram demonstrates that without beam smoothing, a uniform near-field intensity profile picks up phase aberrations along the laser chain, leading to interference and thus large scale modulations at focus. Phase plates are an array of small optical elements which offset the phase of the beam at discrete points in the near-field, acting to shift the scale of modulation in the far-field to a much smaller spatial scale [59]. These short-scale modulations are known as ‘laser-speckle’, and are much more easily smoothed in the conduction zone, than the large modulations from beams without smoothing techniques applied. The static phase plate far-field profile can be further improved by using SSD, which creates a temporally varying speckle pattern and thus the time-integrated profile is much smoother. Fig. 1.8 compactly displays how SSD operates, which is to apply a temporally varying bandwidth to the light signal, then pass it through a diffraction grating, such that different wavelengths are dispersed in different directions [60, 61]. Finally, Polarisation smoothing is employed on OMEGA, which works by splitting each beam into two slightly spatially-offset, orthogonally polarised sub-beams. These sub-beams do not interfere with each other, and thus when added together the root-mean-square intensity variation of the whole beam is improved by a factor $\sqrt{2}$ [62, 63].

Although the combination of these optics create an intensity spot which is smooth when time-integrated, instantaneously large amplitude, short wavelength perturbations exist. When an extended plasma corona has formed, these perturbations are effectively smoothed by non-radial thermal conduction in the conduction zone, but early in the implosion, the small amplitude perturbations are deposited close to the ablation surface. This is known as ‘laser imprint’ and unless mitigated by sufficiently raising the adiabat of the implosion, can break up the shell. The adiabat is typically set for direct-drive implosion by including a small ‘picket’ pulse in the laser temporal profile, which weakly shocks the shell. The laser turns off after this picket pulse, leading to an unsupported shock, which decays in amplitude as it travels through the shell, such that only the outer extent of the shell, where the imprint occurs, is on a high adiabat. Imprint does not occur in indirectly-driven implosion, and thus the highest performing direct-drive experiments normally have much higher adiabats.

LPIs also act to significantly degrade direct-drive ICF implosions. A schematic diagram of LPIs relevant to direct-drive is shown in Fig. 1.9. Energy is absorbed either via Inv-Brem, which is the absorption of laser energy by an electron while it undergoes a collision with an ion, or by resonance absorption, which is the excitation of a resonant EPW at the critical surface. Inv-Brem is the dominant absorption mechanism for OMEGA experiments, because frequency-tripled⁷ light is employed for the lasers, and the Inv-Brem rate scales with frequency of the light [64]. Similarly to indirect-drive, SBS and SRS act to reflect laser light away from the capsule. However, unlike for indirect-drive, where CBET is used to tune the symmetry of the implosion, in direct-drive configurations CBET acts to reflect significant amounts of energy. For direct-drive, the dominant CBET interaction occurs as light from the edge of

⁷The OMEGA laser-beam are initially generated at a vacuum wavelength, $\lambda_0 = 1064$ nm, by a Nd:YAG crystal and then passed through a non-linear optic, which converts the wavelength to $\lambda_0^{3\omega} = 351$ nm [56].

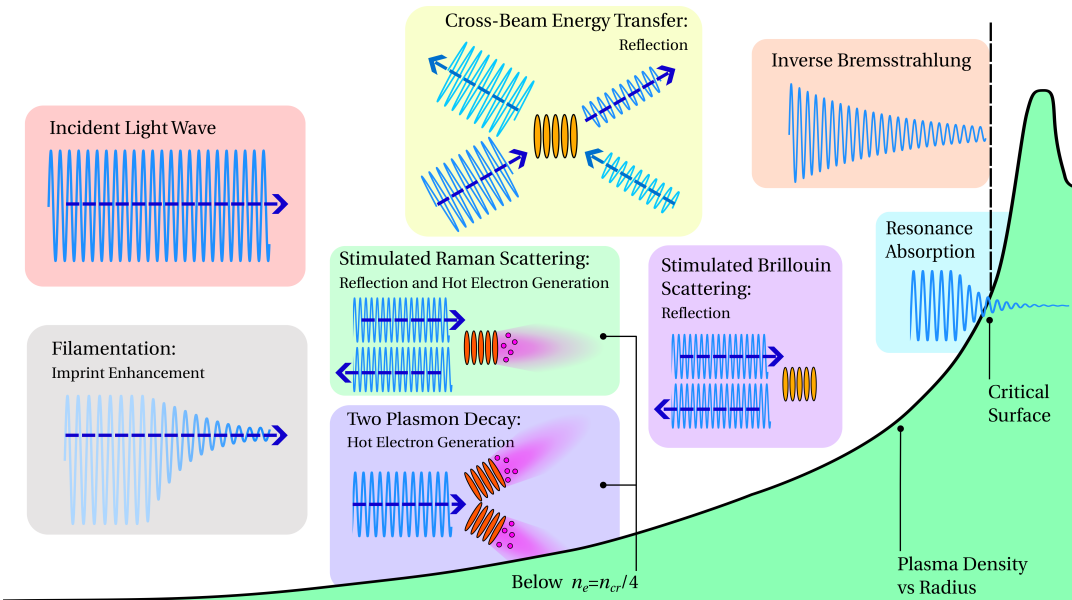


Figure 1.9: Important laser-plasma interactions for direct-drive ICF. Energy is absorbed by Inverse-Bremsstrahlung (Inv-Brem) close to critical, and resonance absorption at the critical surface. Hot electrons pre-heat the fuel, reducing compressibility and are generated from an Electron Plasma Wave (EPW) from Two Plasmon Decay (TPD) or SRS. Energy is reflected by CBET, SRS and SBS. The filamentation instability can cause light to self-focus and thus enhance asymmetry of the deposition. It also raises intensity of the light locally, enhancing the growth rate of other LPIs.

beams reflects outward and gains energy from inward travelling beams. This mechanism is responsible for a $\sim 20\%$ reduction in energy for typical OMEGA implosions over the whole implosion, and can instantaneously reduce power deposition by up to $\sim 50\%$ [65]. Additionally, LPIs which excite an EPW, specifically TPD and SRS, can trap and accelerate a population of electrons to high energies ($\gtrsim 50$ keV), which travel through the ablator material and preheat the fuel, reducing compressibility and thus performance. Finally, filamentation of the beam can occur, where the field self-focusses through low-density channels in the plasma, which increases laser non-uniformities [66].

1.3.2.2 Direct-Drive Experimental Progress

In a central hotspot ICF implosion, fusion reactions are made possible by a sufficiently hot and dense plasma hotspot, which is confined by the inertia of the target. The energy required to assemble this hot and dense configuration occurs through a series of energy transfers.

- Laser energy is converted to internal energy by absorption in the coronal plasma.
- This energy is coupled to kinetic energy in the shell by thermal conduction in the conduction zone.
- Kinetic energy of the shell stagnates on the axis, resulting in internal energy of the hotspot.

- This internal energy allows fuel reactants to overcome the Coulomb barrier and fuse, releasing binding energy as product kinetic energy.

The overall performance of the implosion scales with the internal energy of the hotspot and can be improved, either by increasing the available driver energy, or by increasing the efficiency of these energy conversions. The OMEGA laser facility has insufficient energy to achieve ignition conditions, thus inferring the performance of equivalent implosions on a larger laser direct-drive facility relies on techniques known as hydrodynamic scaling. A combination of analytical methods and simulations are typically used to extrapolate the performance of OMEGA implosions to NIF energies, $E_d \sim 2$ MJ, in order to compare performance of indirect- and direct-drive experiments [67].

Better hydrodynamic stability of the implosion improves the integrity of the imploding shell. In analogy to a stiff piston compressing a gas, a denser and more uniform shell efficiently converts kinetic energy to internal energy of the hotspot gas, whereas a shell with short wavelength perturbations is effectively less dense and more compressible, decreasing conversion efficiency [68]. Over the past decade, implosion performance improved markedly by using statistical modelling techniques [69], to identify and reduce sources of yield degradation [70]. Primarily by focussing on eliminating these short wavelength instabilities using the statistical model, fusion yield was tripled in a short period of time from 5×10^{13} in 2016, to 1.5×10^{14} in 2018 [71]⁸. The details of the statistical model used are discussed in Sec. ??.

More recently, focus has also turned to increasing the efficiency of the energy conversion through other means. Specifically, a significant fraction of laser energy remains unabsorbed, mostly due to CBET, which can reduce power deposition instantaneously by $\sim 50\%$. CBET has been reduced in recent campaigns via two means. Firstly, 'DT-liners' are an experimental configuration which have increased the outer diameter of the target, reducing the beam overlap and thus CBET, which leads to high implosion velocities [72]. This campaign recently reported for the first time that more fusion energy was produced, than was coupled to the hotspot. [73]. Secondly, a small amount ($\sim 5\%$ by atomic number density) of silicon is now routinely added to the outer CH ablator. This enhances the Inv-Brem absorption of light, reducing the quantity of light that refracts away from the target, to act as a seed for CBET. Additionally, addition of a higher-Z dopant into the ablator, reduces growth rates of many LPIs, limiting the hot electron production. A campaign which optimised the addition of silicon dopant recently demonstrated a hydrodynamically equivalent burning plasma on OMEGA, which is an important milestone on the path to hydrodynamically scaled ignition of a direct-drive target [74].

1.4 Objective of the work

Important physical processes in ICF implosions occur on short time and length-scales, and have high temperatures and densities. Inference of plasma conditions from escaping particles or radiation is thus typically used to understand the implosion dynamics. However,

⁸Improved instability robustness was achieved in these implosions, mostly by limiting the convergence ratio of the implosions.

these methods are limited to measuring emissive volumes at certain times throughout the experiments. Simulations are an important tool, which are used to study ICF experiments at greater spatial and temporal resolution than is allowed for by many diagnostic tools. They can also be used to, for example, extrapolate the performance of experiments to larger facilities, or to help design new experiments [52]. The applicability of simulations does of course depend upon the validity of the models used. Hydrodynamic codes are the workhorse tool, used to simulate entire ICF implosions. The models employed in these codes must therefore be capable of accurately including relevant physical effects on long (\sim ns) timescales, which precludes many high fidelity, although expensive tools.

The aim of the work conducted in this thesis was to improve the modelling of the laser-plasma interactions in the 3-D Magnetohydrodynamics (MHD) code CHIMERA, particularly with a view to more accurately simulating direct-drive ICF experiments. Prior to the work conducted in this thesis, a simple ray-tracing algorithm existed in CHIMERA to model the laser-plasma interaction, although it did not accurately account for refraction of the light. Therefore, a simplified 1-D ray-trace was typically used for direct-drive calculations, where rays travelled radially inward and did not refract away from the target. To improve predictive capability, it was deemed necessary to include a 3-D ray-trace, which accurately modelled the trajectory of laser light through the plasma and accounted for refractive coupling losses.

The discussion of indirect-drive in Sec. 1.3.1 and direct-drive in Sec. 1.3.2 hopefully illustrated that LPIs are a significant concern on current ICF experiments. Particularly CBET in direct-drive is highly energetically significant, reducing the efficiency of laser absorption by $\sim 20\%$ over the whole experiment. Additionally, CBET significantly alters deposition asymmetries [65], and therefore it is crucial to accurately model the interaction, in order to understand the degradation of performance from multi-dimensional effects. Despite this, few multidimensional CBET models exist, which are suitable for direct-drive calculations, and only a single code, IFRIIT, had been integrated to run inline with a 3-D hydrodynamics code [65]. The second aim of the work was therefore to develop a CBET model for the ray-trace which could be employed in direct-drive simulations and run inline with the hydrodynamics.

The remainder of this manuscript is organised as followed:

- Chapter ?? introduces background theoretical material, relevant to the interaction of lasers with plasma in the regime of ICF, with a particular focus on the techniques used in the computational models employed in this thesis. Equations of the Radiative-Hydrodynamics (Rad-Hydro) framework are presented, alongside a discussion of their implementation in the CHIMERA code. A summary of the theory of the interaction of laser light with plasma is then presented. The ray-tracing equations are introduced and their validity domain is discussed. Parametric instabilities, also known as LPIs, are finally discussed, with a particular emphasis on CBET.
- Chapter ?? presents the 3-D laser ray-trace and CBET module, SOLAS, which was developed for the CHIMERA code. Initially, the development of the 3-D ray-trace is presented, which includes details on the initialisation of rays, the grid and the numerical

methods. The field reconstruction algorithm is then detailed, which is necessary to obtain the electric field used for calculating the CBET gain, before the CBET algorithm is introduced. Validation problems are presented throughout, which compare SOLAS to both analytic solutions and higher-fidelity solvers. The chapter concludes with an in-line CBET calculation for a 1-D Rad-Hydro simulation of an OMEGA implosion and a 3-D post-process of CBET induced non-uniformity of deposition.

- Chapter ?? presents the results of series of CHIMERA-SOLAS simulations, which were performed to study the effect of the beam-to-target radius ratio of the uniformity of direct-drive implosions. The simulation configuration used for the study is detailed alongside a set of 1-D tuning simulations to obtain the initial conditions for the 2-D simulations. Trends of stagnation state symmetry both in the presence and absence of CBET are presented and the time-resolved growth of the beam-mode asymmetry is studied.
- Chapter ?? gives results of a set of 2-D CHIMERA-SOLAS simulations, which were performed to understand the indirect effect of magnetisation on CBET in direct-drive implosions. Both magnetised and unmagnetised simulations are presented, with and without the effects of CBET on laser deposition. The main results presented are the asymmetries of the stagnation state, for various levels of magnetisation and treatments of CBET.
- Chapter ?? summarises the work conducted in this manuscript and outlines plans for future work, such as potential extensions of the model.

Appendices

Bibliography

- [1] Ember Institute. *Statistical Review of World Energy*. May 2024. URL: <https://ember-climate.org/app/uploads/2024/05/Report - Global - Electricity - Review - 2024.pdf>.
- [2] Thomas Griffiths et al. “The Commercialisation of Fusion for the Energy Market: A Review of Socio-Economic Studies”. In: *Progress in Energy* 4.4 (Oct. 2022), p. 042008. ISSN: 2516-1083. DOI: 10.1088/2516-1083/ac84bf.
- [3] Stefano Atzeni and Jürgen Meyer-ter-Vehn. *The Physics of Inertial Fusion: Beam Plasma Interaction, Hydrodynamics, Hot Dense Matter*. Oxford Science Publications 125. Oxford : New York: Clarendon Press ; Oxford University Press, 2004. ISBN: 978-0-19-856264-1.
- [4] Todd H. Rider. “A General Critique of Inertial-Electrostatic Confinement Fusion Systems”. In: *Physics of Plasmas* 2.6 (June 1995), pp. 1853–1872. ISSN: 1070-664X, 1089-7674. DOI: 10.1063/1.871273.
- [5] M.B. Chadwick et al. “ENDF/B-VII.1 Nuclear Data for Science and Technology: Cross Sections, Covariances, Fission Product Yields and Decay Data”. In: *Nuclear Data Sheets* 112.12 (Dec. 2011), pp. 2887–2996. ISSN: 00903752. DOI: 10.1016/j.nds.2011.11.002.
- [6] Lowell S. Brown and Gerald M. Hale. “Field Theory of the $d + t \rightarrow n + \alpha$ Reaction Dominated by a ${}^5\text{He}^*$ Unstable Particle”. In: *Physical Review C* 89.1 (Jan. 2014), p. 014622. ISSN: 0556-2813, 1089-490X. DOI: 10.1103/PhysRevC.89.014622.
- [7] W. Daughton et al. “Influence of Mass Ablation on Ignition and Burn Propagation in Layered Fusion Capsules”. In: *Physics of Plasmas* 30.1 (Jan. 2023), p. 012704. ISSN: 1070-664X, 1089-7674. DOI: 10.1063/5.0129561.
- [8] Paul-Henri Rebut. “The Joint European Torus (JET)”. In: *The European Physical Journal H* 43.4-5 (Dec. 2018), pp. 459–497. ISSN: 2102-6459, 2102-6467. DOI: 10.1140/epjh/e2017-70068-y.
- [9] John Nuckolls et al. “Laser Compression of Matter to Super-High Densities: Thermonuclear (CTR) Applications”. In: *Nature* 239.5368 (Sept. 1972), pp. 139–142. ISSN: 0028-0836, 1476-4687. DOI: 10.1038/239139a0.
- [10] A. L. Schawlow and C. H. Townes. “Infrared and Optical Masers”. In: *Physical Review* 112.6 (Dec. 1958), pp. 1940–1949. ISSN: 0031-899X. DOI: 10.1103/PhysRev.112.1940.
- [11] T. H. Maiman. “Stimulated Optical Radiation in Ruby”. In: *Nature* 187.4736 (Aug. 1960), pp. 493–494. ISSN: 0028-0836, 1476-4687. DOI: 10.1038/187493a0.

- [12] J. H. Nuckolls Llnl. *Early Steps toward Inertial Fusion Energy (IFE) (1952 to 1962)*. Tech. rep. UCRL-ID-131075, 658936. June 1998, UCRL-ID-131075, 658936. DOI: 10.2172/658936.
- [13] G. S. Fraley et al. “Thermonuclear Burn Characteristics of Compressed Deuterium-Tritium Microspheres”. In: *The Physics of Fluids* 17.2 (Feb. 1974), pp. 474–489. ISSN: 0031-9171. DOI: 10.1063/1.1694739.
- [14] Aidan Crilly. “Simulation of Nuclear Observables in Inertial Confinement Fusion Experiments”. PhD thesis. London: Imperial College London, Apr. 2020. URL: <https://inspirehep.net/literature/1850910> (visited on 09/05/2024).
- [15] M. Lafon et al. “Direct-Drive-Ignition Designs with Mid- Z Ablators”. In: *Physics of Plasmas* 22.3 (Mar. 2015), p. 032703. ISSN: 1070-664X, 1089-7674. DOI: 10.1063/1.4914835.
- [16] J. L. Kline et al. “First Beryllium Capsule Implosions on the National Ignition Facility”. In: *Physics of Plasmas* 23.5 (May 2016), p. 056310. ISSN: 1070-664X, 1089-7674. DOI: 10.1063/1.4948277.
- [17] S. X. Hu et al. “Laser-Direct-Drive Fusion Target Design with a High- Z Gradient-Density Pusher Shell”. In: *Physical Review E* 108.3 (Sept. 2023), p. 035209. ISSN: 2470-0045, 2470-0053. DOI: 10.1103/PhysRevE.108.035209.
- [18] D. T. Casey et al. “Performance and Mix Measurements of Indirect Drive Cu-Doped Be Implosions”. In: *Physical Review Letters* 114.20 (May 2015), p. 205002. ISSN: 0031-9007, 1079-7114. DOI: 10.1103/PhysRevLett.114.205002.
- [19] V. N. Goncharov et al. “Improved Performance of Direct-Drive Inertial Confinement Fusion Target Designs with Adiabat Shaping Using an Intensity Picket”. In: *Physics of Plasmas* 10.5 (May 2003), pp. 1906–1918. ISSN: 1070-664X, 1089-7674. DOI: 10.1063/1.1562166.
- [20] O. A. Hurricane et al. “The High-Foot Implosion Campaign on the National Ignition Facility”. In: *Physics of Plasmas* 21.5 (May 2014), p. 056314. ISSN: 1070-664X, 1089-7674. DOI: 10.1063/1.4874330.
- [21] M. Gatu Johnson et al. “Impact of Asymmetries on Fuel Performance in Inertial Confinement Fusion”. In: *Physical Review E* 98.5 (Nov. 2018), p. 051201. ISSN: 2470-0045, 2470-0053. DOI: 10.1103/PhysRevE.98.051201.
- [22] V A Smalyuk et al. “Review of Hydrodynamic Instability Experiments in Inertially Confined Fusion Implosions on National Ignition Facility”. In: *Plasma Physics and Controlled Fusion* 62.1 (Jan. 2020), p. 014007. ISSN: 0741-3335, 1361-6587. DOI: 10.1088/1361-6587/ab49f4.
- [23] R. Betti et al. “Shock Ignition of Thermonuclear Fuel with High Areal Density”. In: *Physical Review Letters* 98.15 (Apr. 2007), p. 155001. ISSN: 0031-9007, 1079-7114. DOI: 10.1103/PhysRevLett.98.155001.

- [24] L. J. Perkins et al. "Shock Ignition: A New Approach to High Gain Inertial Confinement Fusion on the National Ignition Facility". In: *Physical Review Letters* 103.4 (July 2009), p. 045004. ISSN: 0031-9007, 1079-7114. DOI: 10.1103/PhysRevLett.103.045004.
- [25] R. H. H. Scott et al. "Shock-Augmented Ignition Approach to Laser Inertial Fusion". In: *Physical Review Letters* 129.19 (Nov. 2022), p. 195001. ISSN: 0031-9007, 1079-7114. DOI: 10.1103/PhysRevLett.129.195001.
- [26] Max Tabak et al. "Ignition and High Gain with Ultrapowerful Lasers*". In: *Physics of Plasmas* 1.5 (May 1994), pp. 1626–1634. ISSN: 1070-664X, 1089-7674. DOI: 10.1063/1.870664.
- [27] L. C. Jarrott et al. "Visualizing Fast Electron Energy Transport into Laser-Compressed High-Density Fast-Ignition Targets". In: *Nature Physics* 12.5 (May 2016), pp. 499–504. ISSN: 1745-2473, 1745-2481. DOI: 10.1038/nphys3614.
- [28] T. Gong et al. "Direct Observation of Imploded Core Heating via Fast Electrons with Super-Penetration Scheme". In: *Nature Communications* 10.1 (Dec. 2019), p. 5614. ISSN: 2041-1723. DOI: 10.1038/s41467-019-13574-8.
- [29] Rasol Khoda-Bakhsh et al. "Advanced Fusion Fuel for Inertial Confinement Fusion". In: *Fusion Technology* 22.1 (Aug. 1992), pp. 50–55. ISSN: 0748-1896. DOI: 10.13182/FST92-A30053.
- [30] Kim Molvig et al. "Low Fuel Convergence Path to Direct-Drive Fusion Ignition". In: *Physical Review Letters* 116.25 (June 2016), p. 255003. ISSN: 0031-9007, 1079-7114. DOI: 10.1103/PhysRevLett.116.255003.
- [31] Saumyabrata Banerjee et al. "DiPOLE: A 10 J, 10 Hz Cryogenic Gas Cooled Multi-Slab Nanosecond Yb:YAG Laser". In: *Optics Express* 23.15 (July 2015), p. 19542. ISSN: 1094-4087. DOI: 10.1364/OE.23.019542.
- [32] Dimitri Batani et al. "Future for Inertial-Fusion Energy in Europe: A Roadmap". In: *High Power Laser Science and Engineering* 11 (2023), e83. ISSN: 2095-4719, 2052-3289. DOI: 10.1017/hpl.2023.80.
- [33] V. N. Goncharov et al. "Novel Hot-Spot Ignition Designs for Inertial Confinement Fusion with Liquid-Deuterium-Tritium Spheres". In: *Physical Review Letters* 125.6 (Aug. 2020), p. 065001. ISSN: 0031-9007, 1079-7114. DOI: 10.1103 / PhysRevLett . 125 . 065001.
- [34] I. V. Igumenshchev et al. "Proof-of-Principle Experiment on the Dynamic Shell Formation for Inertial Confinement Fusion". In: *Physical Review Letters* 131.1 (July 2023), p. 015102. ISSN: 0031-9007, 1079-7114. DOI: 10.1103/PhysRevLett.131.015102.
- [35] N. Metzler and J. Meyer-Ter-Vehn. "Target Study for Heavy Ion Beam Fusion". In: *Laser and Particle Beams* 2.1 (Feb. 1984), pp. 27–48. ISSN: 0263-0346, 1469-803X. DOI: 10.1017/S0263034600000604.

- [36] John Lindl. "Development of the Indirect-Drive Approach to Inertial Confinement Fusion and the Target Physics Basis for Ignition and Gain". In: *Physics of Plasmas* 2.11 (Nov. 1995), pp. 3933–4024. ISSN: 1070-664X, 1089-7674. DOI: 10.1063/1.871025.
- [37] George H. Miller. "The National Ignition Facility". In: *Optical Engineering* 43.12 (Dec. 2004), p. 2841. ISSN: 0091-3286. DOI: 10.1117/1.1814767.
- [38] M. L. Spaeth et al. "Description of the NIF Laser". In: *Fusion Science and Technology* 69.1 (Feb. 2016), pp. 25–145. ISSN: 1536-1055, 1943-7641. DOI: 10.13182/FST15-144.
- [39] Noël Fleurot et al. "The Laser Mégajoule (LMJ) Project Dedicated to Inertial Confinement Fusion: Development and Construction Status". In: *Fusion Engineering and Design* 74.1-4 (Nov. 2005), pp. 147–154. ISSN: 09203796. DOI: 10.1016/j.fusengdes.2005.06.251.
- [40] D. S. Clark et al. "Three-Dimensional Simulations of Low Foot and High Foot Implosion Experiments on the National Ignition Facility". In: *Physics of Plasmas* 23.5 (May 2016), p. 056302. ISSN: 1070-664X, 1089-7674. DOI: 10.1063/1.4943527.
- [41] B. J. MacGowan et al. "Laser–Plasma Interactions in Ignition-Scale Hohlraum Plasmas". In: *Physics of Plasmas* 3.5 (May 1996), pp. 2029–2040. ISSN: 1070-664X, 1089-7674. DOI: 10.1063/1.872000.
- [42] P. Michel et al. "Tuning the Implosion Symmetry of ICF Targets via Controlled Crossed-Beam Energy Transfer". In: *Physical Review Letters* 102.2 (Jan. 2009), p. 025004. ISSN: 0031-9007, 1079-7114. DOI: 10.1103/PhysRevLett.102.025004.
- [43] J. D. Moody et al. "Multistep Redirection by Cross-Beam Power Transfer of Ultrahigh-Power Lasers in a Plasma". In: *Nature Physics* 8.4 (Apr. 2012), pp. 344–349. ISSN: 1745-2473, 1745-2481. DOI: 10.1038/nphys2239.
- [44] A. L. Kritcher et al. "Energy Transfer between Lasers in Low-Gas-Fill-Density Hohlraums". In: *Physical Review E* 98.5 (Nov. 2018), p. 053206. ISSN: 2470-0045, 2470-0053. DOI: 10.1103/PhysRevE.98.053206.
- [45] H. Abu-Shwareb et al. "Achievement of Target Gain Larger than Unity in an Inertial Fusion Experiment". In: *Physical Review Letters* 132.6 (Feb. 2024), p. 065102. ISSN: 0031-9007, 1079-7114. DOI: 10.1103/PhysRevLett.132.065102.
- [46] O. A. Hurricane et al. "Physics Principles of Inertial Confinement Fusion and U.S. Program Overview". In: *Reviews of Modern Physics* 95.2 (June 2023), p. 025005. ISSN: 0034-6861, 1539-0756. DOI: 10.1103/RevModPhys.95.025005.
- [47] John Lindl et al. "Review of the National Ignition Campaign 2009–2012". In: *Physics of Plasmas* 21.2 (Feb. 2014), p. 020501. ISSN: 1070-664X, 1089-7674. DOI: 10.1063/1.4865400.
- [48] A. J. MacKinnon et al. "High-Density Carbon Ablator Experiments on the National Ignition Facility". In: *Physics of Plasmas* 21.5 (May 2014), p. 056318. ISSN: 1070-664X, 1089-7674. DOI: 10.1063/1.4876611.

- [49] A. B. Zylstra et al. "Record Energetics for an Inertial Fusion Implosion at NIF". In: *Physical Review Letters* 126.2 (Jan. 2021), p. 025001. ISSN: 0031-9007, 1079-7114. DOI: 10.1103/PhysRevLett.126.025001.
- [50] A. L. Kritchler et al. "Design of the First Fusion Experiment to Achieve Target Energy Gain $G > 1$ ". In: *Physical Review E* 109.2 (Feb. 2024), p. 025204. ISSN: 2470-0045, 2470-0053. DOI: 10.1103/PhysRevE.109.025204.
- [51] A. B. Zylstra et al. "Burning Plasma Achieved in Inertial Fusion". In: *Nature* 601.7894 (Jan. 2022), pp. 542–548. ISSN: 0028-0836, 1476-4687. DOI: 10.1038/s41586-021-04281-w.
- [52] A. L. Kritchler et al. "Design of Inertial Fusion Implosions Reaching the Burning Plasma Regime". In: *Nature Physics* 18.3 (Mar. 2022), pp. 251–258. ISSN: 1745-2473, 1745-2481. DOI: 10.1038/s41567-021-01485-9.
- [53] H. Abu-Shawareb et al. "Lawson Criterion for Ignition Exceeded in an Inertial Fusion Experiment". In: *Physical Review Letters* 129.7 (Aug. 2022), p. 075001. ISSN: 0031-9007, 1079-7114. DOI: 10.1103/PhysRevLett.129.075001.
- [54] *NIF Sets Power and Energy Records | National Ignition Facility & Photon Science*. URL: <https://lasers.llnl.gov/about/keys-to-success/nif-sets-power-energy-records> (visited on 09/06/2024).
- [55] A. Simon. *LLE Review Quarterly Report (April-June 1989). Volume 39*. Tech. rep. DOE/DP/40200-95, 1191446. June 1989, DOE/DP/40200-95, 1191446. DOI: 10.2172/1191446.
- [56] T. R. Boehly et al. "The Upgrade to the OMEGA Laser System". In: *Review of Scientific Instruments* 66.1 (Jan. 1995), pp. 508–510. ISSN: 0034-6748, 1089-7623. DOI: 10.1063/1.1146333.
- [57] M. Gatu Johnson et al. "Impact of Stalk on Directly Driven Inertial Confinement Fusion Implosions". In: *Physics of Plasmas* 27.3 (Mar. 2020), p. 032704. ISSN: 1070-664X, 1089-7674. DOI: 10.1063/1.5141607.
- [58] Stephen E. Bodner. "Critical Elements of High Gain Laser Fusion". In: *Journal of Fusion Energy* 1.3 (July 1981), pp. 221–240. ISSN: 0164-0313, 1572-9591. DOI: 10.1007/BF01050355.
- [59] Y. Kato et al. "Random Phasing of High-Power Lasers for Uniform Target Acceleration and Plasma-Instability Suppression". In: *Physical Review Letters* 53.11 (Sept. 1984), pp. 1057–1060. ISSN: 0031-9007. DOI: 10.1103/PhysRevLett.53.1057.
- [60] S. Skupsky et al. "Improved Laser-Beam Uniformity Using the Angular Dispersion of Frequency-Modulated Light". In: *Journal of Applied Physics* 66.8 (Oct. 1989), pp. 3456–3462. ISSN: 0021-8979, 1089-7550. DOI: 10.1063/1.344101.
- [61] M. Hohenberger et al. "Optical Smoothing of Laser Imprinting in Planar-Target Experiments on OMEGA EP Using Multi-FM 1-D Smoothing by Spectral Dispersion". In: *Physics of Plasmas* 23.9 (Sept. 2016), p. 092702. ISSN: 1070-664X, 1089-7674. DOI: 10.1063/1.4962185.

- [62] K. Tsubakimoto et al. "Suppression of Interference Speckles Produced by a Random Phase Plate, Using a Polarization Control Plate". In: *Optics Communications* 91.1-2 (July 1992), pp. 9–12. ISSN: 00304018. DOI: 10.1016/0030-4018(92)90091-5.
- [63] T. R. Boehly et al. "Reduction of Laser Imprinting Using Polarization Smoothing on a Solid-State Fusion Laser". In: *Journal of Applied Physics* 85.7 (Apr. 1999), pp. 3444–3447. ISSN: 0021-8979, 1089-7550. DOI: 10.1063/1.369702.
- [64] J Huba D. *NRL Plasma Formulary*. Tech. rep. NRL/PU/6790-13-589. Washington, DC: Naval Research Laboratory, 2013.
- [65] A. Colaïtis et al. "Inverse Ray Tracing on Icosahedral Tetrahedron Grids for Non-Linear Laser Plasma Interaction Coupled to 3D Radiation Hydrodynamics". In: *Journal of Computational Physics* 443 (Oct. 2021), p. 110537. ISSN: 0021-9991. DOI: 10.1016/j.jcp.2021.110537.
- [66] T. Afshar-rad et al. "Evidence for Whole-Beam Self-Focusing of Induced Spatially Incoherent Laser Light in Large Underdense Plasma". In: *Physical Review Letters* 68.7 (Feb. 1992), pp. 942–945. ISSN: 0031-9007. DOI: 10.1103/PhysRevLett.68.942.
- [67] C. D. Zhou and R. Betti. "Hydrodynamic Relations for Direct-Drive Fast-Ignition and Conventional Inertial Confinement Fusion Implosions". In: *Physics of Plasmas* 14.7 (July 2007), p. 072703. ISSN: 1070-664X, 1089-7674. DOI: 10.1063/1.2746812.
- [68] R. Betti et al. "Deceleration Phase of Inertial Confinement Fusion Implosions". In: *Physics of Plasmas* 9.5 (May 2002), pp. 2277–2286. ISSN: 1070-664X, 1089-7674. DOI: 10.1063/1.1459458.
- [69] A. Lees et al. "Experimentally Inferred Fusion Yield Dependencies of OMEGA Inertial Confinement Fusion Implosions". In: *Physical Review Letters* 127.10 (Aug. 2021), p. 105001. ISSN: 0031-9007, 1079-7114. DOI: 10.1103/PhysRevLett.127.105001.
- [70] A. Lees et al. "Understanding the Fusion Yield Dependencies in OMEGA DT-layered Implosion Experiments Using a Physics-Based Statistical Mapping Model". In: *Physics of Plasmas* 30.1 (Jan. 2023), p. 012709. ISSN: 1070-664X, 1089-7674. DOI: 10.1063/5.0106515.
- [71] V. Gopalaswamy et al. "Tripled Yield in Direct-Drive Laser Fusion through Statistical Modelling". In: *Nature* 565.7741 (Jan. 2019), pp. 581–586. ISSN: 0028-0836, 1476-4687. DOI: 10.1038/s41586-019-0877-0.
- [72] C. A. Williams et al. "High Yields in Direct-Drive Inertial Confinement Fusion Using Thin-Ice DT Liner Targets". In: *Physics of Plasmas* 28.12 (Dec. 2021), p. 122708. ISSN: 1070-664X, 1089-7674. DOI: 10.1063/5.0069372.
- [73] C. A. Williams et al. "Demonstration of Hot-Spot Fuel Gain Exceeding Unity in Direct-Drive Inertial Confinement Fusion Implosions". In: *Nature Physics* 20.5 (May 2024), pp. 758–764. ISSN: 1745-2481. DOI: 10.1038/s41567-023-02363-2.

- [74] V. Gopalswamy et al. “Demonstration of a Hydrodynamically Equivalent Burning Plasma in Direct-Drive Inertial Confinement Fusion”. In: *Nature Physics* 20.5 (May 2024), pp. 751–757. ISSN: 1745-2473, 1745-2481. DOI: 10.1038/s41567-023-02361-4.

Permissions